Acta Pharmaceutica Sinica B 2022;12(3):1447−1459

Chinese Pharmaceutical Association
Institute of Materia Medica, Chinese Academy of Medical Sciences

Acta Pharmaceutica Sinica B

www.elsevier.com/locate/apsb
www.sciencedirect.com

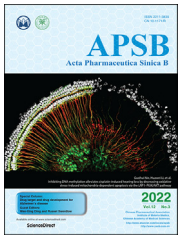

ORIGINAL ARTICLE

Chemo-photothermal immunotherapy for eradication of orthotopic tumors and inhibition of metastasis by intratumoral injection of polydopamine versatile hydrogels

Bo Zhuang[a,b], Ting Chen[a], Yueqi Huang[a], Zhimei Xiao[a], Yiguang Jin[a,*]

[a]*Department of Pharmaceutical Sciences, Beijing Institute of Radiation Medicine, Beijing 100850, China*
[b]*Department of Chemical Defense, Institute of NBC Defense, Beijing 102205, China*

Received 26 May 2021; received in revised form 8 July 2021; accepted 2 August 2021

KEY WORDS

Breast cancer;
Polydopamine;
Hydrogel;
Intratumoral injection;
Photothermal;
Chemotherapy;
Immunotherapy;
Metastasis

Abstract Cancer remains one of the leading causes of death globally and metastasis always leads to treatment failure. Here, we develop a versatile hydrogel loading photothermal agents, chemotherapeutics, and immune-adjuvants to eradicate orthotopic tumors and inhibit metastasis by combinational therapy. Hydrogel networks were synthesized *via* the thiol-Michael addition of polydopamine (PDA) with thiolated hyaluronic acid. PDA acted as a cross-linking agent and endowed the hydrogel with excellent photothermal property. Meanwhile, a chemotherapeutic agent, doxorubicin (DOX), was loaded in the hydrogel *via* $\pi-\pi$ stacking with PDA and an immune-adjuvant, CpG-ODN, was loaded *via* electrostatic interaction. The release of DOX from the hydrogel was initially slow but accelerated due to near infrared light irradiation. The hydrogels showed remarkably synergistic effect against 4T1 cancer cells and stimulated plenty of cytokines secreting from RAW264.7 cells. Moreover, the hydrogels eradicated orthotopic murine breast cancer xenografts and strongly inhibited metastasis after intratumoral injection and light irradiation. The high anticancer efficiency of this chemo-photothermal immunotherapy resulted from the strong synergistic effect of the versatile hydrogels, including the evoked host immune response. The

Abbreviations: ALT, alanine aminotransferase; CCK-8, cell counting kit-8; CRE, creatinine; DOX, doxorubicin; DOX@PDA, DOX-loaded PDA nanoparticles; DTT, dithiothreitol; EDC, 1-ethyl-3-(3-dimethylaminopropyl) carbodiimide; ELISA, enzyme-linked immunosorbent assay; FBS, fetal bovine serum; FDA, fluorescein diacetate; HA, hyaluronic acid; HA-SH, thiolated hyaluronic acid; H&E, Hematoxylin and Eosin; LPS, lipopolysaccharide; NHS, *N*-hydroxysuccinimide; NIR, near-infrared; PDA, polydopamine; PI, propidium iodide; PTT, photothermal therapy; RBC, red blood cells; SEM, scanning electron microscope; Tunel, terminal deoxynucleotidyl transferase dUTP nick end labeling; WBC, white blood cells.

*Corresponding author. Tel.: +86 10 88215159; fax: +86 10 68214653.
E-mail address: jinyg@sina.com (Yiguang Jin).

Peer review under responsibility of Chinese Pharmaceutical Association and Institute of Materia Medica, Chinese Academy of Medical Sciences.

https://doi.org/10.1016/j.apsb.2021.09.001

combinational strategy of chemo-photothermal immunotherapy is promising for highly effective treatment of breast cancer.

1. Introduction

Despite the advances in the diagnosis and treatment of human malignancy, cancer remains among the leading causes of morbidity and mortality worldwide[1]. Recently, female breast cancer has surpassed lung cancer as the most commonly diagnosed cancer[2]. Clinical treatments of primary breast cancer include surgery, radiotherapy, and chemotherapy. However, metastasis happens in the early stage of breast cancer and mainly contributes to breast cancer-related death, which cannot be treated well with the traditional treatments leading to a low five-year survival rate of 22%[3,4]. Therefore, a comprehensive treatment strategy is urgently needed for the treatment of primary breast cancer and its metastasis.

Nowadays, immunotherapy is recognized as the most powerful weapon to win the battle against cancer[5,6]. Immunotherapy evokes and trains the immune system to fight against cancer including circulating cancer cells and micro-metastasis. Several kinds of cancer immunotherapies, such as chimeric antigen receptor T-cell, checkpoint-blockade therapy, cytokine therapy, cancer vaccines and so forth, have been established and achieved exciting results in clinical trials[7,8]. However, the clinical application of immunotherapy is limited with individual variations in therapeutic responses, nonspecific inflammation, autoimmunity, and extremely high costs[9]. Thus, a combinational strategy is required to address the limitations.

Photothermal therapy (PTT) becomes an increasingly recognized alternative for cancer therapy with high selectivity and extremely low invasiveness[10−12]. More importantly, the damaged tumor tissues by PTT would likely release tumor-related antigens that can be recognized by the immune system[10,13,14]. Under the help of checkpoint blockade, vaccine-like tumor antigens boost the immune system to fight against metastatic cancer cells in the circulation and distant tissues and relieves immune suppression of the tumor[15,16]. PTT involves photothermal agents and light irradiation. However, the clinical applications of photothermal agents, *e.g.*, inorganic nanomaterials and organic dyes[17,18], are limited owing to concerns on their long-term safety and/or photobleaching[19−21]. Polydopamine (PDA) is the primary component of melanin as an excellent PTT agent due to its good biocompatibility, tissue adhesion, and high photo-stability[22−24]. Therefore, we focus on preparation of a novel type of PDA-based formulations for PTT. However, only PTT-induced tumor-related immune response may be weak, not producing enough strong eradication of cancer cells in the whole body.

Chemotherapy is still the most common cancer treatment strategy, which is often combined with other therapeutic ways, such as immunotherapy and PTT. It is now accepted that certain chemotherapies can augment tumor immunity by inducing immunogenic cell death as part of its intended therapeutic effect and by disrupting strategies that tumors use to evade immune recognition[16,25]. In addition, hyperthermia can enhance the cytotoxicity of chemotherapeutic agents so that the synergistic antitumor effect of PTT and chemotherapy is achieved[26,27]. Topical chemo-photothermal therapy is beneficial to eradicate primary tumor tissues due to the concentrated distribution of killing factors[28−30]. However, localized chemo-photothermal therapy is helpless for lethal metastasis, which needs the systemic tumor specific immune response to conquer metastasis.

Here, we designed a new anti-breast cancer formulation combining chemotherapy, PTT, and immunology, which not only eradicates the primary breast tumor but also strongly inhibits the distant metastasis. PDA is the matrix and modified to form versatile hydrogels loading chemotherapeutics and immune-adjuvants. The three functions are realized with this formulation after intratumoral (i.t.) injection to the orthotopic breast tumor tissues. Besides the direct killing effect of chemo-photothermal therapy, the outstanding feature of this treatment is the production of tumor-related antigens. The addition of immune-adjuvants amplifies the self-immune response of tumor-related antigens to inhibit distant metastasis. The PDA-based versatile hydrogel is suitable for i.t. injection with an on-demand drug release profile. A bilateral breast cancer animal model was established for the pharmacodynamic study. The highly efficient synergistic anticancer effect of this versatile hydrogel was demonstrated after comparison between the combinational therapy and the monotherapies and the mechanisms were discovered.

2. Materials and methods

2.1. Materials

Sodium salt of hyaluronic acid (HA, 150 kDa, 96%) was purchased from Yangzhou Joyvo WeiKem Biology Co., Ltd. (Yangzhou, China). Doxorubicin hydrochloride (DOX) was obtained from Ark Pharm Inc. (Chicago, USA). 1-Ethyl-3-(3-dimethylaminopropyl) carbodiimide (EDC), *N*-hydroxysuccinimide (NHS), cystamine dihydrochloride and dopamine hydrochloride were provided by Beijing InnoChem Science & Technology Co., Ltd. (Beijing, China). Purified water was prepared using Heal Force Super NW Water System (Shanghai Canrex Analytic Instrument Co., Ltd., Shanghai, China). All other reagents were of analytical grade without further purification. Fetal bovine serum (FBS), Roswell Park Memorial Institute (RMPI 1640), Dulbecco's modified Eagle's medium (DMEM) and trypsin−EDTA were purchased from Gibco Life Technologies (USA). Cell Counting Kit-8 (CCK-8) was purchased from Gen-view Scientific Inc. (USA). Both fluorescein diacetate (FDA) and propidium iodide (PI) were purchased from Sinopharm Chemical Reagent Co., Ltd. (Shanghai, China). TNF-α, IL-6, IFN-γ ELISA kits were purchased from Neobioscience Co., Ltd. (Shenzhen, China).

2.2. Cells and animals

A normal fibroblast cell line from mouse (L929), a luciferase tagged murine breast cancer cell line (4T1-luc) and a mouse monocyte/

macrophage cell line (RAW264.7) were purchased from the Cell Bank of the Chinese Academy of Sciences (Shanghai, China).

Female BALB/c mice (18−20 g) were purchased from Beijing Vital River Laboratory Animal Technology Co., Ltd. (Beijing, China). All experimental procedures were executed according to the protocols approved by Animal Care and Use Committee at Academy of Military Medical Science.

2.3. Synthesis and characterization of thiolated hyaluronic acid

Thiolated hyaluronic acid (HA-SH) was synthesized by a facile two-step synthetic procedure that involved amidation of HA with cystamine dihydrochloride and subsequent disulfide bond cleavage[31]. Firstly, 1 mmol of HA was dissolved in 100 mL of water. Afterwards, EDC (3 mmol) and NHS (3 mmol) were successively added. The mixture was immediately adjusted to pH 5.5 using 0.1 mol/L HCl solution. Then, a series of cystamine dihydrochloride (0.5, 1, and 3 mmol) were parallelly added. After agitation for 24 h at room temperature, the mixture was dialyzed (MWCO 3500 Da) against water for 24 h to remove residues. Next, 0.5 g of dithiothreitol (DTT) was added to cleave the disulfide bond at pH 8.5. The crude product of HA-SH was purified by dialysis. To avoid the oxidation of thiol groups, dialysis was conducted at 4 °C and pH 5.0. Finally, the HA-SH solution was lyophilized. The ^{1}H NMR spectra of HA-SH were recorded with JEOL NMR spectrometer (400 MHz, Akishima, Japan) after dissolution in D_2O. In addition, the thiol content was quantified with the Ellman method[32].

2.4. Preparation and characterization of PDA

PDA was obtained by the oxidative self-polymerization of dopamine hydrochloride[33]. Briefly, a series of ammonia aqueous solutions (28%−30%) of 0.4, 0.8, 1.2, and 1.6 mL were added to a mixture of ethanol (16 mL) and water (36 mL) under mild agitation, respectively. A dopamine hydrochloride solution (0.05 g/mL, 4 mL) was added dropwise and reacted for 24 h. The black product was collected by centrifugation (14,800×g, 10 min, H2-16 KR, Hunan Kecheng Instrument Equipment Co., Ltd., Changsha, China) and washed with water.

The size distribution and zeta potential of PDA were analyzed with a particle size analyzer (Nano ZS, Malvern Instruments, Worcestershire, UK). The microscale morphologies of PDA nanoparticles were observed under a transmission electron microscopy (TEM, H-7650, 80 kV, Hitachi, Tokyo, Japan) after negative staining of the samples with a phosphotungstic acid solution (pH 7.0).

2.5. Preparation and characterization of PDA/HA-Gel

PDA/HA-Gel was formed after the Michael addition of PDA with HA-SH. An HA-SH solution (15 mg/mL) and a PDA suspension (10 mg/mL) were prepared, respectively. The two solutions were 1:1 mixed and the mixture self-formed hydrogels at 37 °C. PDA/HA-Gel was freeze-dried and sliced up for microstructure assay. A slice was coated with a thin layer of gold on the cross-sections and observed under a scanning electron microscope (SEM, S-4800, 5 kV, Hitachi, Tokyo, Japan).

The biocompatibility of PDA/HA-Gel was investigated in terms of cytotoxicity, hemolysis, and systemic toxicity of mouse. The cytotoxic experiment of gel materials was conducted on L929 cells. An erythrocyte suspension was incubated with the hydrogel for 1 h to examine hemolysis. The *in vivo* biocompatibility of PDA/HA-Gel was explored by subcutaneous injection of the gels into the back of mice. The body weight, blood count, and blood chemistry were analyzed at predetermined time points.

The rheological properties of PDA/HA-Gel were determined with an Anton Paar MCR302 rheometer (Graz, Austria). Storage modulus (G″) and loss modulus (G′) were recorded. The oscillatory strain sweep experiments of gels were conducted at a constant frequency of 10 rad/s and the strain varied from 0.1 to 1000. The gels formed after 0, 2, and 6 h were used to investigate the rheological properties.

2.6. In vitro photothermal effect

The photothermal effect of PDA suspensions and PDA/HA-Gel were investigated under near-infrared (NIR) irradiation. The samples were placed in quartz cuvette and irradiated with a 780 nm NIR laser (Yuanming Lasever, Ningbo, China) at a power density of 1.3 W/cm^2 for 10 min, and the temperature was recorded using a contact thermometer (HT-9815, Xintest, Shenzhen, China) and an infrared thermal camera (FOTRIC 220s, Fotric Thermal Intelligence, USA).

2.7. Preparation and characterization of versatile hydrogels

DOX was absorbed on the surface of PDA nanoparticles *via* π−π stacking. DOX solutions (4 mg/mL) and PDA suspensions (20 mg/mL) were 1:1 mixed followed by 12 h agitation in dark. DOX-loaded PDA nanoparticles (DOX@PDA) were collected by centrifugation (14,800×g, 10 min, Kecheng Instrument) and washed 3 times with water. The size and zeta potential of DOX@PDA were analyzed. The visible absorption spectra of DOX@PDA were conducted with the UV−Vis spectrophotometer (TU-1901, Beijing Purkinje General Instrument Co., Ltd., Beijing, China). For hydrogel preparation, DOX@PDA suspension (10 mg/mL) was incubated with CpG-ODN solution and then cross-linked with an HA-SH solution (15 mg/mL). Six hours post-gelation, a versatile hydrogel was formed and named as CpG@DOX@PDA-Gel.

2.8. Release and diffusion of DOX

DOX@PDA-Gel (1 cm^3, containing 1 mg DOX) was immersed in PBS (pH = 7.4, 8 mL) with or without HAase. At predetermined time points (Days 1, 3, 6, 9, 12, and 15), 4 mL of the release media was withdrawn for measurement and equal volume of fresh PBS was supplemented. DOX in the media was determined with spectrophotometry (Purkinje Instrument). In addition, the drug release behavior was also investigated under NIR irradiation. The hydrogels were irradiated with a 780 nm-NIR laser (Yuanming Lasever) at a power density of 1.3 W/cm^2 for 10 min followed by an interval of 50 min. The procedure was performed 5 times.

We prepared a solid hydrogel to roughly simulate tumor stroma for investigation of drug diffusion. The diffusion behavior of the injectable hydrogel in the simulated tumor matrix was photographed at predetermined time points. Meanwhile, DOX solution and DOX@PDA suspension served as controls.

2.9. Evaluation of cell viability and cytokines after chemo-photothermal therapy

In vitro antitumor effect of chemo-photothermal therapy was evaluated with the cell counting kit-8 (CCK-8) assay. 4T1-luc

cells (5000 cells/well) were seeded into a 96-well plate and cultured overnight. The cells were incubated with the media supplemented with PDA and DOX@PDA at a series of concentration for 4 h. The PTT groups were exposed to NIR irradiation at 1.0 W/cm^2 for 5 min. The cells were further incubated for 20 h until measurement of cell viability as the instruction of CCK-8 assay. Furthermore, the antitumor effect was also studied using the live/dead assay[34]. 4T1-luc cells were seeded in a 6-well plate. Twelve hours later, the media were withdrawn and the cells were covered with the PDA-Gel or DOX@PDA-Gel. Then, the culture media were added into the wells for standard incubation. Four hours later, the cells were exposed to NIR (1.3 W/cm^2 × 8 min). After 12 h incubation, the cells were washed with PBS and stained with FDA (5 μg/mL) and PI (5 μg/mL) at room temperature for 5 min in the dark. The cells were thoroughly washed with PBS before observation under a Nikon TiE-A1 confocal laser scanning microscope (Tokyo, Japan).

The cytokines released from RAW 264.7 cells were determined with an enzyme-linked immunosorbent assay (ELISA) method[35]. 4T1-luc cells and RAW 264.7 cells were separately seeded into 24-well culture plates at a density of 2 × 10^5 cells per well. Twelve hours later, the 4T1-luc cells were incubated with CpG@PDA and CpG@DOX@PDA, where the final concentrations of PDA, DOX and CpG-ODN were 0.5 mg/mL, 1 μmol/L, and 0.5 μmol/L, respectively. Four hours later, the 4T1-luc cells were irradiated with an NIR laser device (1.3 W/cm^2 × 10 min, Yuanming Lasever). The media of 4T1-luc cells were transferred to the plates seeded with RAW 264.7 cells followed by incubation for 24 h. Afterwards, the media of RAW 264.7 cells were centrifuged (14,800×*g*, 20 min, Kecheng Instrument) and the supernatants were collected for cytokines determination. The contents of TNF-α and IL-6 were determined with ELISA kits.

2.10. Measurements of in vivo antitumor effect and immune response

Orthotopic breast tumor models were established by the transplantation of 1 × 10^6 4T1-luc cells into the mammary fat pads of mice. When the tumor volume reached ~100 mm^3, the mice were randomly divided into six groups (n = 12 per group). They were separately treated as follows: (1) the model group without treatment, (2) the PDA-Gel group without NIR irradiation, (3) the PDA-Gel group with NIR irradiation, (4) the DOX@PDA-Gel group with NIR irradiation, (5) the CpG@PDA-Gel group with NIR irradiation, (6) the CpG@DOX@PDA-Gel group with NIR irradiation. The compositions of hydrogels were listed in Supporting Information Table S1. The treatment groups were i.t. injected with 0.1 mL of the hydrogels. The needle was moved in the tumor tissues for uniform distribution of the hydrogels. The tumor area was irradiated with a 780-nm NIR laser (1.0 W/cm^2 × 5 min, Yuanming Lasever) 12 h post-injection and the photothermal imaging was recorded with an infrared thermal camera. A week later, the residual tumor was irradiated with NIR again. The treatment lasted for two weeks. During treatment, the bioluminescence of tumors was monitored with an *in vivo* imaging system (IVIS, Lumina II, caliper life sciences, Waltham, MA, USA). Body weight and tumor volume were recorded every three days. Tumor volume was calculated as length × width^2 × 0.5. To examine the antitumor immune response, the cytokines in the serum and cytotoxic T cells in the spleen were investigated. Three days post-PTT, peripheral blood was obtained by retro-orbital blood collection and centrifuged to separate serum for cytokine assay. Then, the mice were euthanized and the spleens were excised. The spleen cells were collected except red blood cells and stained with CD3e and CD8 antibodies. The fluorescence was analyzed with a flow cytometer (BD II, BD Biosciences, Franklin Lakes, NJ, USA). Finally, the mice were euthanized and the tumors and the major organs were excised, fixed in formalin, dehydrated, and paraffin embedded. The samples were sectioned and stained with hematoxylin and eosin (H&E), caspase-3 and terminal deoxynucleotidyl transferase dUTP nick end labeling (Tunel).

2.11. Inhibition of distant metastatic tumor

A bilateral tumor model was used to investigate the metastatic tumor inhibition. 4T1-luc cells (1 × 10^6) were inoculated into the right mammary fat pad of mice to form the primary tumor. Three days later, 5 × 10^5 4T1-luc cells were injected into the left mammary fat pad to form a distant metastatic tumor. The primary tumors were treated with CpG@PDA-Gel plus NIR irradiation. In addition, one group was administrated with anti-PDL1 *via* tail vein for 3 times at time interval of 3 days. The inhibition of metastatic tumor was evaluated in terms of tumor volume and immunohistochemistry.

2.12. Statistical analysis

All data were expressed as mean ± standard deviation (SD). The results were calculated statistically using the SPSS 19.0 software (SPSS, Chicago, IL, USA). One-way analysis of variance (ANOVA) with the LSD test was used to identify differences ($P < 0.05$ or $P < 0.001$) between the data.

3. Results and discussion

3.1. Characteristics of HA-SH and PDA

HA is one of the most versatile and fascinating macromolecules in the natural world. It can be modified with various functional moieties to form functional hydrogels[36]. Here, HA-SH was successfully synthesized. HA-SH showed a significant different NMR spectrum from HA with a new signal at 2.75 ppm (a, HS–CH_2–, Supporting Information Fig. S1), which was attributed to the grafted cysteamine[37]. The thiol substitution degree in HA-SH (*vs.* the disaccharide units of HA) was 8.47, 10.20 and 11.32% when reaction with 0.5, 1, 3 equivalent moles of cystamine, respectively. Thus, the thiol substitution could be tuned to form hydrogel with different crosslink density. The HA-SH with 10.20% thiol substitution degree was used for hydrogel preparation. The average molecular weight of HA was 150 kDa. Accordingly, the molecular weight of HA-SH was approximately calculated as 152,180 Da. The molecular weight represents the chain length of HA-SH and the thiol substitution degree, which has an important influence on the gelation behavior.

The TEM image revealed that PDA was spherical nanoparticles (Fig. 1A). The diameter depended on the ammonia concentration in the reaction system. The diameter had a steep decrease from 712 to 149 nm when the ammonia amount increased from 0.4 to 1.6 mL in the system; meanwhile, the yield decreased from 24.5% to 7.6% (Supporting Information Table S2). We chose PDA at size of 226 nm for further study, in which case the yield was 11.5%. The size distribution of a representative PDA was shown in Fig. 1B and the peak value was 206 nm, while the zeta potential measured in neutral aqueous solution was −21.3 mV (Fig. 1C).

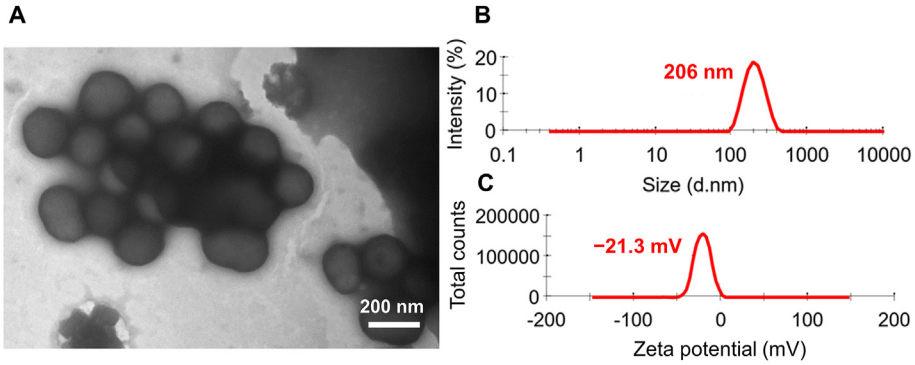

Figure 1 Characteristics of PDA. TEM image (A), size distribution (B), and zeta potential (C) of PDA.

The surface charge on PDA is probably due to quinone imine and catechol groups, which can strongly depend on the measurement conditions (pH, electrolyte)[38].

3.2. *Characteristics of HA/PDA-Gel*

HA-SH and PDA were the two precursors of HA/PDA-Gel and they cross-linked due to the Michael reaction. HA/PDA-Gel did not flow after gelation for 2 h (Fig. 2A). The SEM images revealed that the hydrogel contained a high density of PDA dispersed in the matrix (Fig. 2B), which was a reasonable observation because PDA acted as cross-linker to form hydrogel.

The rheological properties reflected viscosity, elasticity, and mechanical strength of HA/PDA-Gel. The G″ represents the solid properties of the gel, and the G′ represents the fluid properties of the gel. A fully developed gel or "strong gel" has the property of $G'' > G'$[39]. When tested at 0 h, both of G″ and G′ were less than 10 Pa (Fig. 2C), indicating the mixture was in a sol state. After gelation for 2 h, G″ increased to about 100 Pa (Fig. 2D) and then reached about 500 Pa after 6 h (Fig. 2E), which indicated the gel strength increased gradually as cross-linking reaction proceeded. The gel formed by Michael reaction has a long curing time, and the low gel strength in the initial phase is suitable for injection. The composite viscosity of PDA/HA-Gel decreased rapidly as the amplitude increased and finally approached to zero (Fig. 2F), which is easy to inject for lower viscosity under high shear.

Biosafety is a critical precondition for biomedical application of materials. Neither HA-SH nor PDA had an effect on the proliferation of L929 cells (Supporting Information Fig. S2A and S2B). No hemolysis activity was observed when the erythrocytes incubated with the hydrogel, confirming high blood compatibility of HA/PDA-Gel (Fig. S2C). The body weight of HA/PDA-Gel implanted mice continually increased, showing a similar profile to the healthy ones (Fig. S2D). Moreover, the white blood cells (WBC), red blood cells (RBC), alanine aminotransferase (ALT), and creatinine (CRE) showed no difference between the hydrogel-bearing mice and the healthy ones (Supporting Information Fig. S3). The hyaluronic acid would be degraded by enzyme and polydopamine nanoparticles would be phagocytized by macrophages and degraded under acid conditions, such as lysosome[40,41]. Taken together, HA/PDA-Gel possesses excellent biocompatibility and biodegradation and has potential for biomedical application.

3.3. *High photothermal conversion ability*

PDA converts light to heat with high efficiency. The electrons in PDA are excited by light energy and the following non-radiative relaxation generates heat[42]. The temperature of PDA suspensions rose quickly under NIR irradiation. The temperature of PDA at concentration of 100 μg/mL reached about 60 °C after irradiation for 10 min (Fig. 3A). Moreover, the photothermal effect still led to the same climactic temperature after three cycles of NIR irradiation, suggesting an excellent photothermal stability (Fig. 3B). It provides the probability for multiple PTT. In addition, the HA/PDA-Gel also exhibited good photothermal effect thanks to the embedded PDA. The hydrogel's temperature surpassed 60 °C with the PDA concentration of 1 or 5 mg/mL (Fig. 3C), which was high enough to ablate tumor. Moreover, different types of hydrogels were injected into the tumor site, and the temperature was measured by infrared camera under NIR irradiation. The temperature rapidly surpassed 55 °C after 5 min regardless of drug loaded in HA/PDA-Gel (Fig. 3D). The *in vivo* photothermal effect of HA/PDA-Gel was strong enough for tumor ablation. Moreover, the heat focused on the tumor site (Fig. 3F), alleviating side effects of hyperthermia.

3.4. *DOX loaded on PDA via π–π stacking with high efficiency*

The mechanism of drug loaded in carriers has important influence on the therapeutic effect. The main drug loading mechanisms include covalent conjugation or physical encapsulation. However, covalent or physical loading manner shows limits for low loading efficiency or burst releasing, respectively. The π–π stacking interaction, a type of non-covalent interaction, is often used as a strategy for the design of drug-delivery systems, which can enhance therapeutic effect with desirable drug load or release behavior[43]. Thanks to the π electrons-rich structure, DOX could be easily loaded onto PDA by π–π stacking interaction and burst release was avoided. Compared to PDA, the particle size of DOX@PDA grew larger from 206.5 to 269.1 nm (Fig. 4A), attributing to DOX deposition on the surface of PDA. Moreover, the zeta potential of PDA gradually shifted from −34.1 to 17.6 mV due to the cationic structure of amino group in DOX (Fig. 4B). The positive charge promoted CpG-ODN coating on DOX@PDA *via* electrostatic interaction, because CpG-ODN always had negative charge. After DOX was loaded in PDA, the peak absorbance of DOX shifted from 480 to 501 nm (Fig. 4C), moving towards the red part of the spectrum. The red shift was caused by intermolecular π–π conjugation. All these results confirm the DOX loaded onto PDA successfully *via* π–π stacking interaction. By this means, the drug loading efficiency was high and burst release could be avoided.

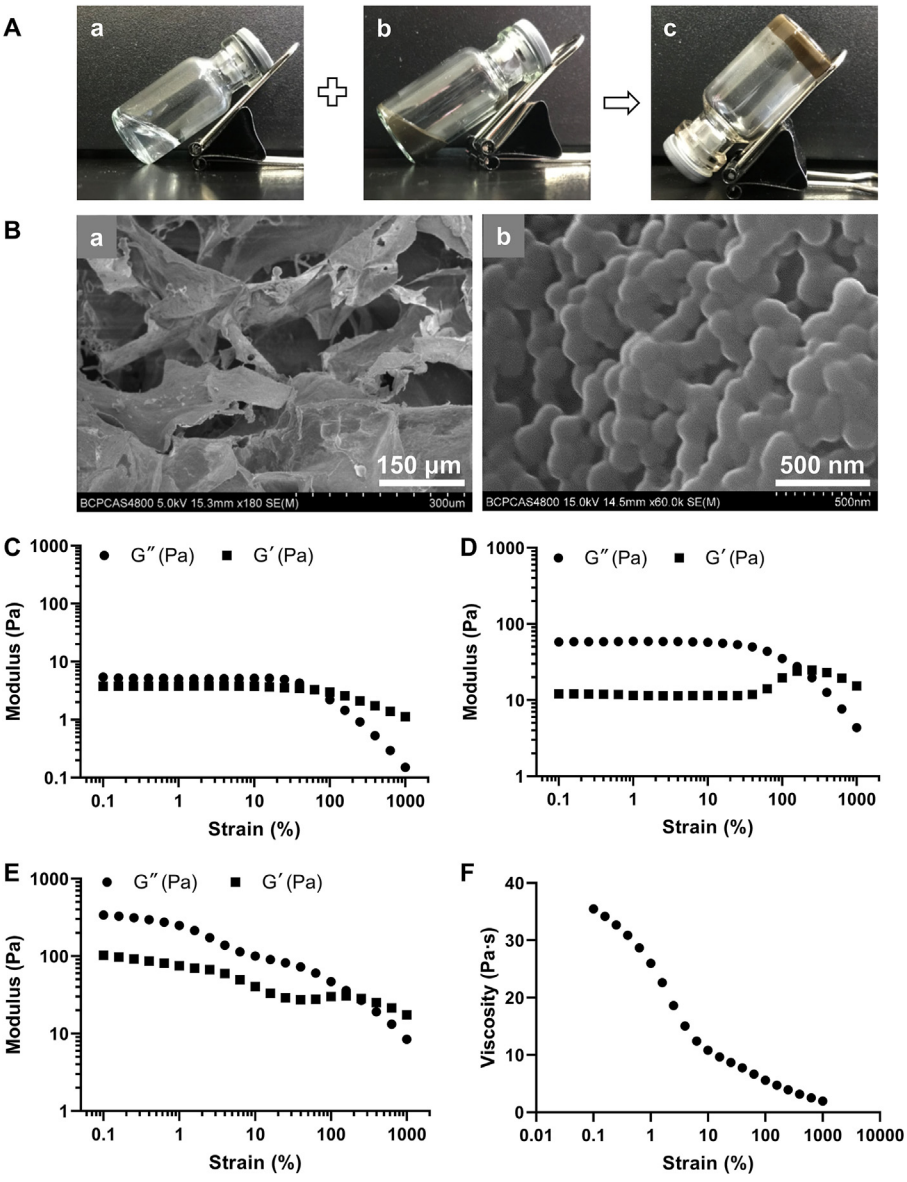

Figure 2 Appearance, microstructure and rheological property of PDA/HA-Gel. (A) Appearance of the hydrogel formation process (a, HA-SH solution; b, PDA suspension; c, solid hydrogel after gelation for 2 h). (B) SEM image of the hydrogel. Amplitude sweep test of hydrogels after gelation for 0 min (C), 2 h (D), and 6 h (E). (F) The composite viscosity of hydrogel after gelation for 6 h. G″ means storage modulus and G′ means loss modulus.

3.5. Controlled DOX release and diffusion behavior

In chemo-photothermal therapy, the main part of tumor was ablated by hyperthermia, and then chemotherapeutics took effect to kill the remaining cancer cells. Long residence time and controlled release profile of chemotherapeutics ensure high efficient elimination of remaining cancer cells. However, the controlled release of hydrophilic drug in hydrogel was a tough nut. Here, DOX loaded onto PDA *via* π–π stacking to avoid fast release, and then cross-linked with HA-SH. DOX slowly released from the hydrogel in PBS within 15 days, while the addition of HAase accelerated drug release obviously (Fig. 5A). The DOX@PDA-Gel degraded rapidly under the help of HAase with shrinking volume and detection of PDA nanoparticles in release media (Supporting Information Fig. S4), denoting enzyme triggered drug release behavior. Moreover, elevated temperature could promote molecular diffusion. Reasonably, DOX released rapidly during NIR irradiation and the release rate recovered to normal without light stimulus (Fig. 5B). It clearly indicated an on-demand drug release behavior. NIR irradiation could facilitate the release of DOX in tumor site, leading to high bioavailability of DOX and synergistic therapeutic effect.

The diffusion behaviors of DOX solution, PDA suspension and PDA-Gel were investigated in tumor stroma-simulated hydrogels. The DOX solution and PDA suspension diffused after 6 h and fulfilled the well after 12 h (Fig. 5C). By contrast, PDA-Gel changed little after injection into simulated tumor matrix, which could prevent drug leakage from the tumor site. Previous paper reported that PDA

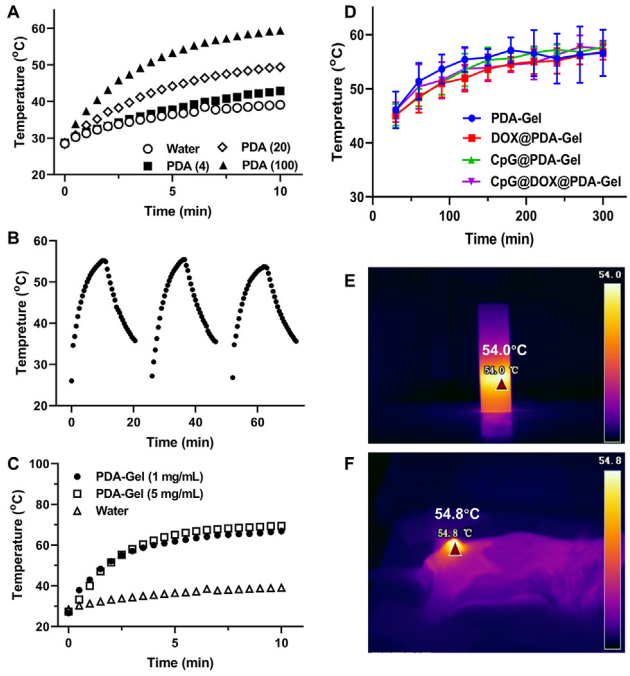

Figure 3 Photothermal effect of PDA and PDA-Gel. (A) Temperature of PDA at different concentration under NIR irradiation. (B) Cyclic temperature rise and fall of PDA. (C) Temperature of PDA-Gel under NIR irradiation. (D) *In vivo* photothermal effect of different formulation of PDA-Gel under NIR irradiation. Data are presented as mean ± SD ($n = 3$). Infrared thermal image of PDA-Gel (E) and tumor-bearing mouse (F).

suspension begin to decrease after 4 h post-injection in the tumor site[44]. Thus, the injectable hydrogel could resident at the tumor site, increasing local drug concentration for long-term.

3.6. *Synergistic anti-proliferation effect of chemo-photothermal therapy against 4T1-luc cells*

The 4T1-luc cells viability was nearly 100% after incubation with PDA (Fig. 6A), indicating high safety of PDA in the dark. By contrast, under NIR irradiation the photothermal effect of PDA

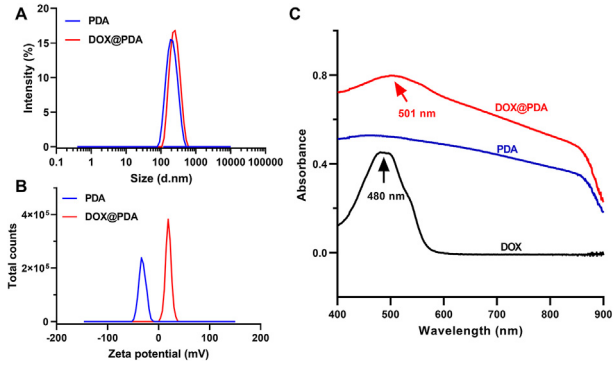

Figure 4 Characteristics of DOX@PDA. Size distribution (A) and zeta potential (B) of PDA and DOX@PDA. (C) UV−Vis absorption spectra of DOX, PDA, and DOX@PDA.

inhibited cell proliferation significantly in a concentration dependent manner (Fig. 6B). Moreover, the DOX@PDA with NIR irradiation, in meaning of chemo-photothermal therapy, inhibited cell proliferation more significantly compared to mono-photothermal therapy at the same condition ($P < 0.05$). Interestingly, the cell viability after incubation with DOX@PDA plus NIR was similar with that after incubation with free DOX, which might be attributed to little DOX released from DOX@PDA in a short time. In consideration of the light sensitivity of DOX, the NIR influence to the anticancer effect of DOX was investigated. The cell viability showed no difference between free DOX group and free DOX + NIR group, indicating that NIR had no influence on the anticancer effect of DOX (Supporting Information Fig. S5).

The *in vitro* antitumor effect of chemo-photothermal therapy was furtherly investigated by live/dead staining. The NIR had no effect on the cell proliferation. Almost all cells kept alive after coverage with PDA-Gel for 12 h without NIR, indicating high cytocompatibility of blank PDA-Gel (Fig. 6C). The DOX@PDA-Gel showed no influence on the cells due to slow drug release and the short intervention time. In the above experiment, the cell viability was approximately 80% under PDA plus moderate NIR irradiation (1.0 W/cm^2 × 5 min). However, when irradiated by strong NIR irradiation (1.3 W/cm^2 × 8 min), almost all the cells in both PDA-Gel and DOX@PDA-Gel group were dead. These results indicated that the photothermal effect could be tuned to ablate tumor or just impair the cancer cells. Then, chemotherapy could subsequently take effect to kill remaining cancer cells in later stage, improving the therapeutic effect synergistically.

3.7. *Cytokines release and inhibition of cell growth*

Photothermal therapy induces tumor-related antigen releasing from cancer cells, such as heat-shock protein and cell debris, while chemotherapy leads to immunogenic cell death[16]. Both of PTT and chemotherapy can trigger anticancer immune responses including dendritic cell maturation and cytokines release. The 4T1-luc cells antigen plus CpG-ODN significantly stimulated TNF-α releasing, which was as high as lipopolysaccharide (LPS) group (Fig. 7A). However, the cytokines secreted by RAW264.7 cells in CpG@PDA(+) and CpG@DOX@PDA(+) groups showed no significant difference ($P > 0.05$). The chemotherapy induced immunogenic cell death might be covered up by intense photothermal effect in short time. The IL-6 showed the same trend between the experimental groups and PTT damage was prerequisite for a mass of cytokines release (Fig. 7B). The secreted cytokines by immune cells not only can promote host immune response to kill cancer cells, but also can directly intervene cancer cell proliferation. The cell culture media of RAW 264.7 cells inhibited 4T1 cell growth (Fig. 7C), and the inhibition rate was in accordance with the amount of released cytokines. Dendritic cell (DC) maturation has been approved to be a pivotal process for initiating immunity[45]. The DC2.4 cells were used to investigate the DC maturation after treatment with CpG@PDA(+), CpG@DOX@PDA(−), and CpG@DOX@PDA(+). The three combination strategies improved the maturation of DC and the most DC maturation appeared in the CpG@DOX@PDA(+) group (Supporting Information Fig. S6). The mature DC would present the antigen to activate T cell response for cancer immunotherapy.

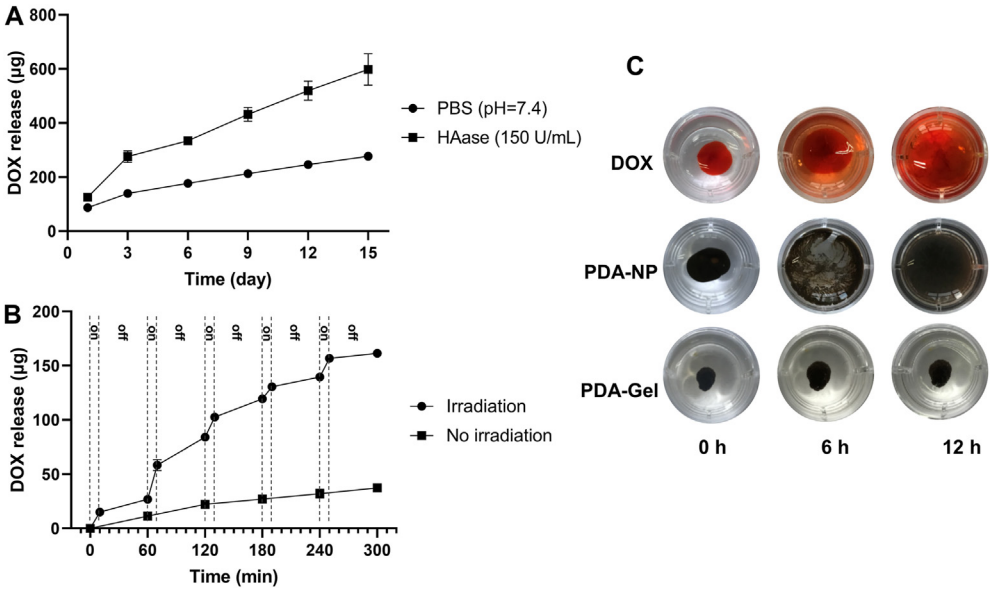

Figure 5 *In vitro* DOX release from PDA-Gel and diffusion behavior of different formulation. (A) DOX release in PBS and HAase solution. (B) DOX release under NIR irradiation. (C) The diffusion behavior of different formulation in simulated tumor matrix. Data are presented as mean ± SD ($n = 3$).

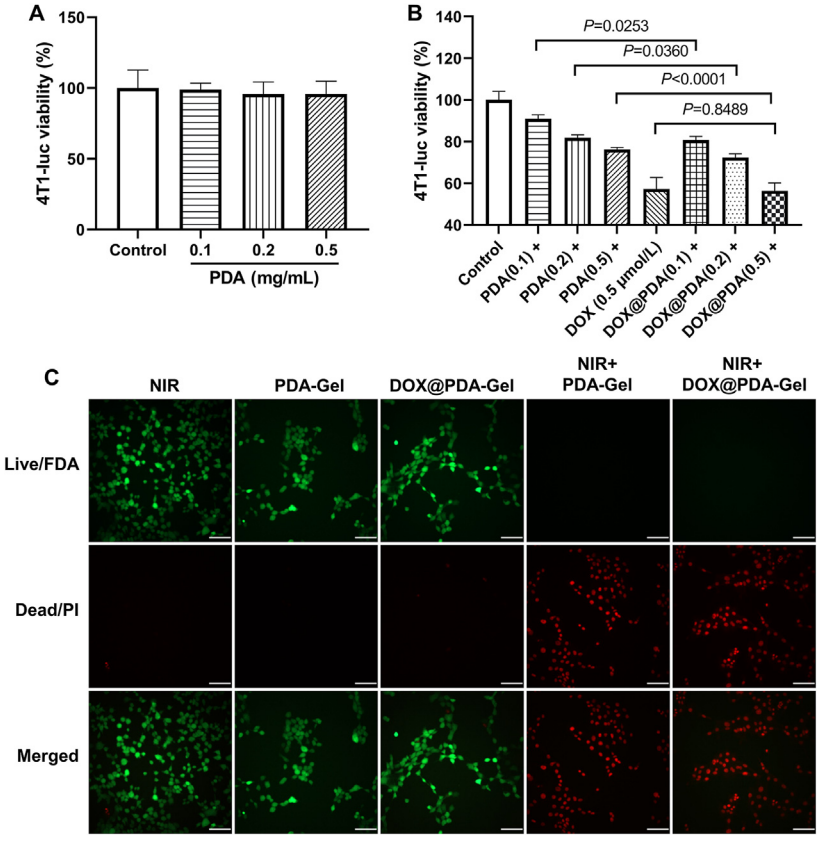

Figure 6 *In vitro* anticancer effect of therapies against 4T1 cells. (A) Cytotoxicity of PDA without NIR irradiation. (B) Cytotoxicity of chemotherapy and PTT ("+" indicates NIR irradiation). (C) Live/dead staining of 4T1-luc cells after chemo-photothermal therapy. Data are presented as mean ± SD ($n = 6$). Scale bar = 100 μm.

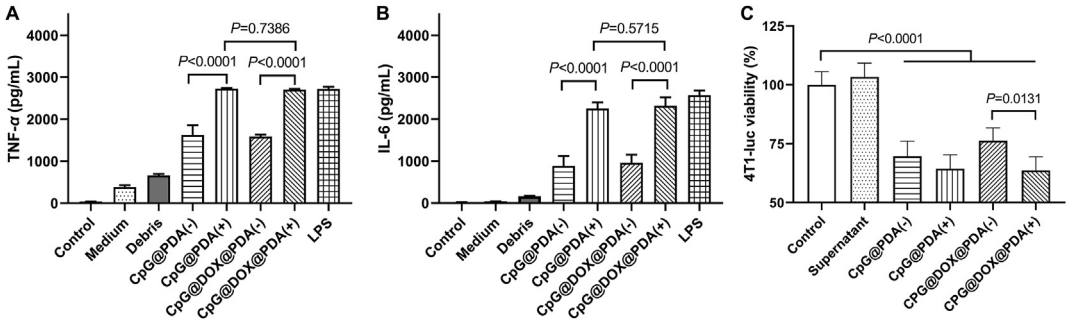

Figure 7 Cytokines released from RAW264.7 cells (A, B) and inhibition of 4T1-luc cells (C). Data are presented as mean ± SD ($n = 5$).

3.8. High host immune response and antitumor effect of chemo-photothermal immunotherapy

The ablative treatments such as hyperthermia could induce strong *in vivo* tumor-specific immune responses[46]. Cytokines took part in the process of immune responses. TNF-α and IL-6 contents in the serum of the CpG@DOX@PDA(+) and CpG@PDA(+) groups were higher than those of the other groups ($P < 0.0001$, Fig. 8A and B), indicating PTT plus immune-adjuvant induced strong immune response. TNF-α is a critical mediator of cellular immunity and IL-6 is a typical marker of humoral immunity, both of which contribute to tumor regression. The spleen is an important immune organ to combat disease. The cancer can cause damaged cells, thereby restricting the spleen from performing its functions. We observed the enlargement of spleen in the model or mono-therapy group, while the splenic size in three-mode combination group almost had no change. Other reports demonstrated that splenic weight doubled for tumor bearing mice[47]. The host immune system could eliminate the cancer cells by $CD3^+/CD8^+$ cytotoxic T lymphocytes. The level of $CD3^+/CD8^+$ T cells in spleen of mice treated by CPG@DOX@PDA(+) and CpG@PDA(+) was higher than the other groups ($P < 0.0001$, Fig. 8C and D). Specifically, after treatment by PTT plus CpG-ODN the cytotoxic T cells in spleen rose to approximately 20% from 11% (in the untreated group). The cytotoxic T lymphocytes can kill cancer cells directly by releasing perforin, granzymes and granulysin[48].

Inspired by the excellent photothermal performance and immune responses of the versatile hydrogel, we investigated

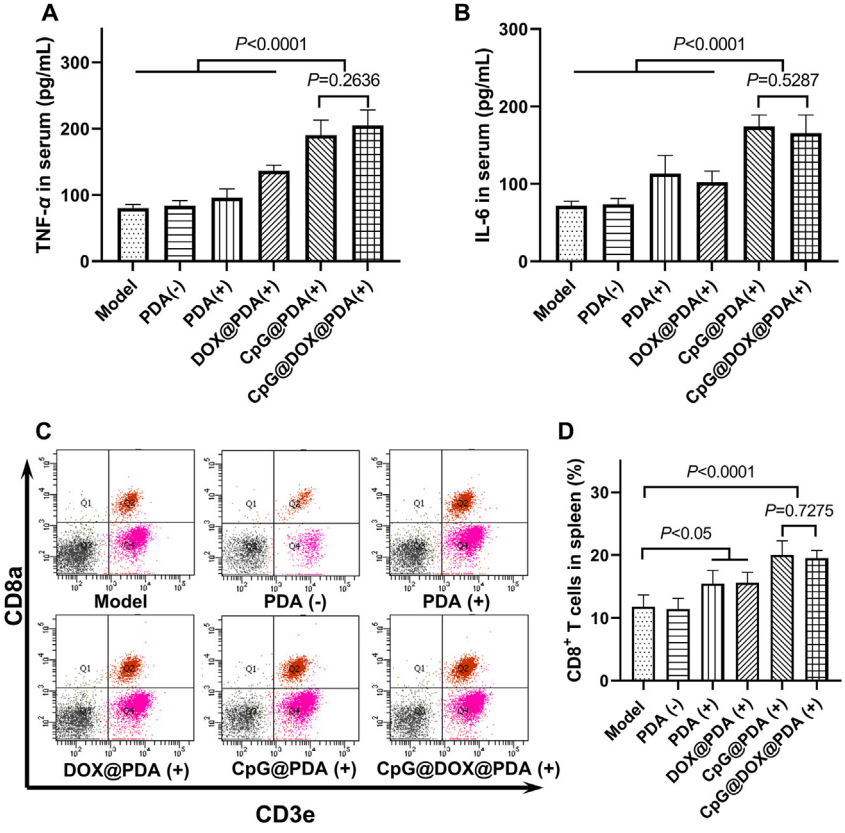

Figure 8 Activity of *in vivo* immune system after various treatment. TNF-α (A) and IL-6 (B) content in peripheral blood serum. (C) CD3 and CD8 staining image of T cells in spleen. (D) Quantitative analysis of $CD3^+/CD8^+$ T cells in spleen. Data are presented as mean ± SD ($n = 3$).

whether those effects could treat tumors. The IVIS images clearly revealed the inhibition of tumor growth (Fig. 9A and B). The fluorescence intensity of tumors after treatment was lower than that in the model or the blank gel group, which meant the therapeutic regimen inhibited tumor growth. After the second irradiation, the antitumor therapeutic effect was enhanced. On Day 12, there was only one fluorescent mouse in the three-mode combination treatment group, exhibiting lowest fluorescence intensity (Fig. 9C). Tumor volume is a direct indicator to reflect the tumor growth. The palpable tumor was ablated by PTT regardless additional treatment regimen. Thus, the tumor volume in all the PTT groups was obviously smaller than that of model

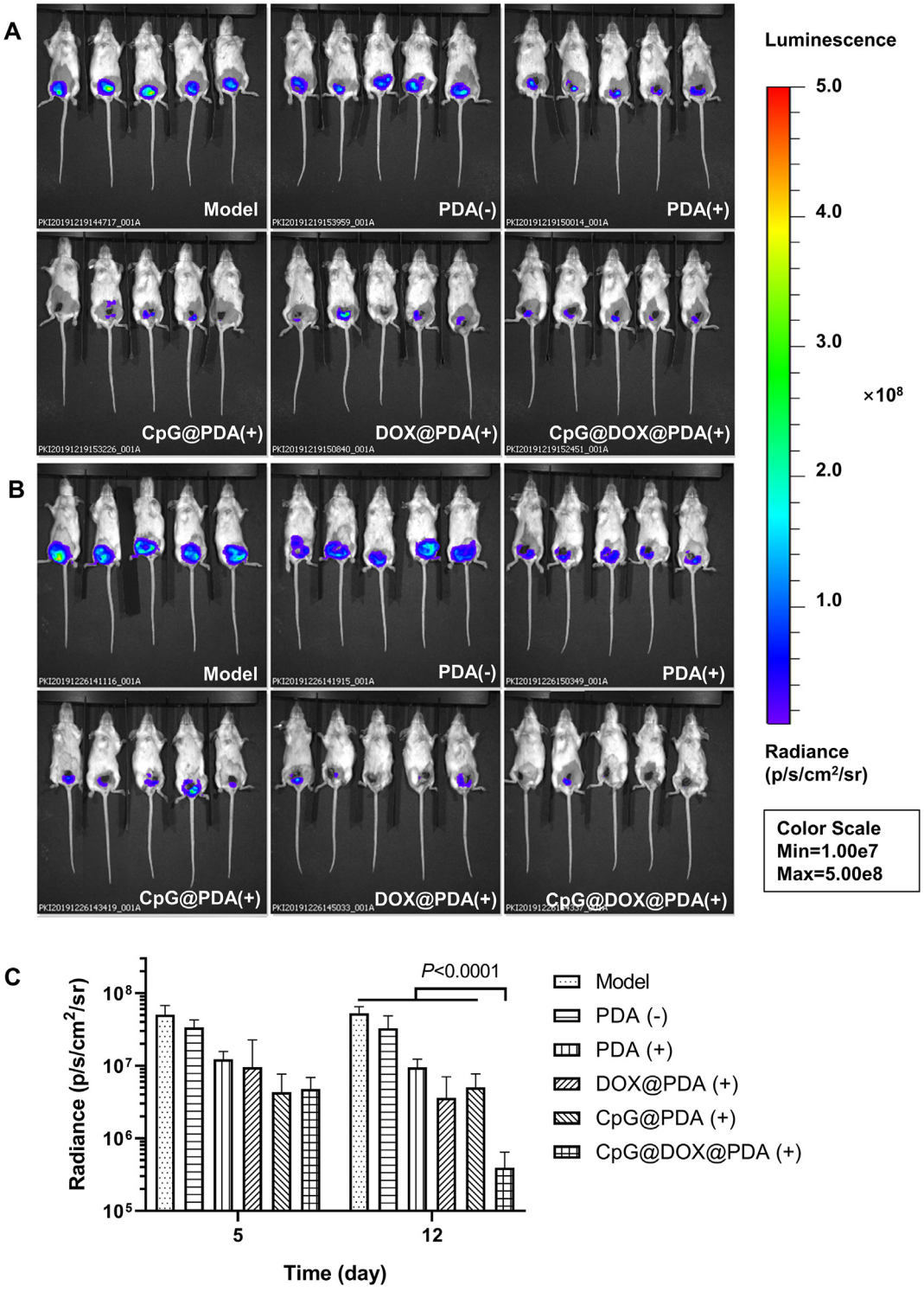

Figure 9 *In vivo* fluorescent image of tumor-bearing mice. IVIS image of mice on Day 5 (A) and Day 12 post-treatment (B). (C) Radiance intensities of tumors after treatment. Data are presented as mean ± SD ($n = 5$).

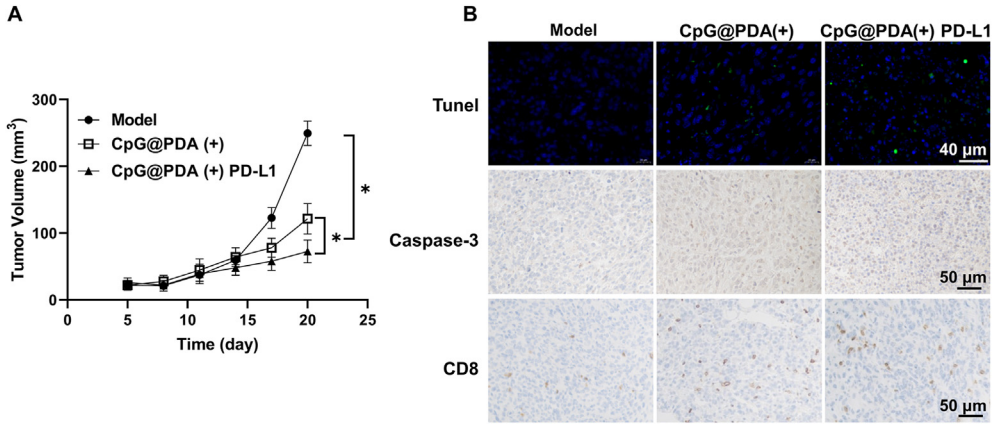

Figure 10 Suppression of metastatic tumor after treatment of primary tumor. (A) Tumor volume of metastatic tumors. (B) Tunel, caspase-3 and CD8 staining of metastatic tumors. Data are presented as mean ± SD ($n = 6$), *$P < 0.05$.

or blank gel group (Supporting Information Fig. S7A). The mouse body weight fluctuated in a small extent (<20%) during the experimental period (Fig. S7B), indicating the treatment regimen had little systemic toxicity. To sum up, the main part of tumor was ablated by PTT and chemotherapeutics were released around the tumor site in a sustained way to kill the remaining cancer cells, and the host immune system was furtherly evoked to contribute to therapeutic outcome. Both the PTT and chemotherapy would induce immunogenic cell death and release tumor-related antigen, such as calprotectin and heat shock protein, acting as *in situ* tumor vaccines[49]. These results show that a three-mode combined strategy was significantly superior to single-mode therapy to treat cancers, paving new avenue for incurable cancer patients.

Pathological investigation and immunohistochemical staining furtherly showed the anticancer effects of different treatment regimen. Tunel staining shows apoptosis cells in the treatment group while the model and the blank gel group had no obvious apoptosis phenomenon (Supporting Information Fig. S8). The chemo-photothermal group (DOX@PDA+) and the three-mode combination group (CpG@DOX@PDA+) had more apoptosis cells, indicating better therapeutic effect. Caspase-3 enzyme is a member of endoproteases family, which regulates inflammation and apoptosis signaling networks. It plays a part in cytotoxic T cells killing cancer cells mechanism[50]. The three-mode combination group showed more caspase-3 positive cells, indicating more apoptosis cells in tumor tissue. Moreover, H&E staining revealed lung metastasis in the model group, while the treatment group showed no metastasis (Supporting Information Fig. S9). There were no obvious damage in heart tissue, which is prone to injury by DOX. The injectable hydrogel show little side effects due to localized drug distribution.

3.9. *Inhibition of distantly metastatic tumor*

Metastasis is the major cause of treatment failure in cancer patients and of cancer-related deaths. Since the therapeutic outcome to treat primary tumor was confirmed, we further investigated the potential of host immune response to suppress cancer metastasis. In the present study, a bilateral tumor model was established by twice inoculation of cancer cells. The bigger tumor served as the primary tumor while the smaller tumor was regarded as a distant metastasis. The metastatic tumor volume was significantly suppressed after the treatment of the primary tumor with CpG@PDA plus laser irradiation (Fig. 10A). Moreover, the tumor volume of mice administrated with additional PD-L1 antibody become significantly lower ($P < 0.05$), indicating the enhanced immune-therapeutic effect with help of anti-PD-L1. In addition, the metastatic tumors showed more positive results in Tunel and caspase-3 staining after treatment of primary tumor plus PD-L1 antibody (Fig. 10B). Moreover, CD8 staining had the same trend, demonstrating more tumor-infiltrating cytotoxic T cells with PD-L1 antibody. In addition, the cytotoxic T cells in the distant tumor were also investigated with a flow cytometer after CD3 and CD8 staining. The CpG@PDA(+) group showed more $CD3^+/CD8^+$ cells than the model group, indicating enhanced immunotherapy to inhibit metastatic tumors (Supporting Information Fig. S10). The host immune response induced by treatment of primary tumor plus PD-L1 antibody could suppress distant metastasis, bringing hope for advanced cancer patients. The PD-L1 antibody avoids the tumor immune escape by blocking the PD-L1 immune checkpoints. However, only PD-L1 antibody showed compromised results for the low host immune response. Moreover, many papers demonstrated the activation of innate and adaptive immune systems by combinational therapy (*e.g.*, PTT or PDT) could significantly improve the therapeutic efficiency of PD-L1 antibody[51,52].

4. Conclusions

Metastasis happens in the earliest tumor proliferation; however, many drug carrier studies focus on the treatment of primary tumors not probable distant metastasis. Here, we developed a combinational therapy of chemo-photothermal immunotherapy, for highly effective anti-primary tumor and distant metastasis treatment at the same time with only once i.t. injection of the versatile hydrogel, *i.e.*, DOX/CpG-ODN-loaded HA/PDA-Gel. The hydrogel was precisely designed based on the physiological and pathological conditions of orthotopic breast tumor and distant metastasis. The high photothermal effect of PDA led to the rapid death of the cancer cells at the orthotopic site. The chemotherapeutic, DOX released to the surrounding tumor tissues with a controllable manner. The combination of the cellular residues of killed cancer cells and CpG-ODN improved the systematic immune response to highly inhibit the proliferation of distant metastatic cancer cells. The versatile hydrogel is a promising medication for highly effective treatment of primary and metastatic tumors.

Acknowledgments

This work was partially supported by the National Natural Science Foundation of China (82073791).

Author contributions

Bo Zhuang and Yiguang Jin designed the research, carried out the experiments and performed data analysis. Ting Chen, Yueqi Huang and Zhimei Xiao participated part of the experiments. Bo Zhuang wrote the manuscript. Yiguang Jin revised the manuscript. All of the authors have read and approved the final manuscript.

Conflicts of interest

The authors declare no conflict of interest in this work.

Appendix A. Supporting information

Supporting data to this article can be found online at https://doi.org/10.1016/j.apsb.2021.09.001.

References

1. Chembiochem Ferlay J, Colombet M, Soerjomataram I, Mathers C, Parkin DM, Piñeros M, et al. Estimating the global cancer incidence and mortality in 2018: GLOBOCAN sources and methods. *Int J Canc* 2019;**144**:1941−53.
2. Sung H, Ferlay J, Siegel RL, Laversanne M, Soerjomataram I, Jemal A, et al. Global cancer statistics 2020: GLOBOCAN estimates of incidence and mortality worldwide for 36 cancers in 185 countries. *CA A Cancer J Clin* 2021;**71**:209−49.
3. Zugazagoitia J, Guedes C, Ponce S, Ferrer I, Molina-Pinelo S, Paz-Ares L. Current challenges in cancer treatment. *Clin Therapeut* 2016;**38**:1551−66.
4. Maeda H, Khatami M. Analyses of repeated failures in cancer therapy for solid tumors: poor tumor-selective drug delivery, low therapeutic efficacy and unsustainable costs. *Clin Transl Med* 2018;**7**:11.
5. Ng CW, Li J, Pu K. Recent progresses in phototherapy-synergized cancer immunotherapy. *Adv Funct Mater* 2018;**28**:1804688.
6. Sugie T. Immunotherapy for metastatic breast cancer. *Chin Clin Oncol* 2018;**7**:28.
7. Riley RS, June CH, Langer R, Mitchell MJ. Delivery technologies for cancer immunotherapy. *Nat Rev Drug Discov* 2019;**18**:175−96.
8. Adams S, Gatti-Mays ME, Kalinsky K, Korde LA, Sharon E, Amiri-Kordestani L, et al. Current landscape of immunotherapy in breast cancer: a review. *JAMA Oncol* 2019;**5**:1205−14.
9. Hegde PS, Chen DS. Top 10 challenges in cancer immunotherapy. *Immunity* 2020;**52**:17−35.
10. Chen Q, Xu L, Liang C, Wang C, Peng R, Liu Z. Photothermal therapy with immune-adjuvant nanoparticles together with checkpoint blockade for effective cancer immunotherapy. *Nat Commun* 2016;**7**:13193.
11. Kim HS, Lee DY. Near-infrared-responsive cancer photothermal and photodynamic therapy using gold nanoparticles. *Polymers* 2018;**10**:961.
12. Sun X, Zhuang B, Zhang M, Jiang H, Jin Y. Intratumorally injected photothermal agent-loaded photodynamic nanocarriers for ablation of orthotopic melanoma and breast cancer. *ACS Biomater Sci Eng* 2019;**5**:724−39.
13. Nam J, Son S, Ochyl LJ, Kuai R, Schwendeman A, Moon JJ. Chemo-photothermal therapy combination elicits anti-tumor immunity against advanced metastatic cancer. *Nat Commun* 2018;**9**:1074.
14. Chen X, Zou J, Zhang K, Zhu J, Zhang Y, Zhu Z, et al. Photothermal/matrix metalloproteinase-2 dual-responsive gelatin nanoparticles for breast cancer treatment. *Acta Pharm Sin B* 2021;**11**:271−82.
15. Wang C, Sun W, Wright G, Wang AZ, Gu Z. Inflammation-triggered cancer immunotherapy by programmed delivery of CpG and anti-PD1 antibody. *Adv Mater* 2016;**28**:8912−20.
16. Fan Y, Kuai R, Xu Y, Ochyl LJ, Irvine DJ, Moon JJ. Immunogenic cell death amplified by co-localized adjuvant delivery for cancer immunotherapy. *Nano Lett* 2017;**17**:7387−93.
17. Jung HS, Verwilst P, Sharma A, Shin J, Sessler JL, Kim JS. Organic molecule-based photothermal agents: an expanding photothermal therapy universe. *Chem Soc Rev* 2018;**47**:2280−97.
18. Lv S, Miao Y, Liu D, Song F. Recent development of photothermal agents (PTAs) based on small organic molecular dyes. *Chembiochem* 2020;**21**:2098−110.
19. Xing R, Liu K, Jiao T, Zhang N, Ma K, Zhang R, et al. An injectable self-assembling collagen-gold hybrid hydrogel for combinatorial antitumor photothermal/photodynamic therapy. *Adv Mater* 2016;**28**:3669−76.
20. Bakalova R, Zhelev Z, Aoki I, Masamoto K, Mileva M, Obata T, et al. Multimodal silica-shelled quantum dots: direct intracellular delivery, photosensitization, toxic, and microcirculation effects. *Bioconjugate Chem* 2008;**19**:1135−42.
21. Xia B, Wang B, Shi J, Zhang Y, Zhang Q, Chen Z, et al. Photothermal and biodegradable polyaniline/porous silicon hybrid nanocomposites as drug carriers for combined chemo-photothermal therapy of cancer. *Acta Biomater* 2017;**51**:197−208.
22. Cheng W, Zeng X, Chen H, Li Z, Zeng W, Mei L, et al. Versatile polydopamine platforms: synthesis and promising applications for surface modification and advanced nanomedicine. *ACS Nano* 2019;**13**:8537−65.
23. Zhao L, Bi D, Qi X, Guo Y, Yue F, Wang X, et al. Polydopamine-based surface modification of paclitaxel nanoparticles for osteosarcoma targeted therapy. *Nanotechnology* 2019;**30**:255101.
24. Chen R, Zhu C, Fan Y, Feng W, Wang J, Shang E, et al. Polydopamine-based multifunctional platform for combined photothermal therapy, chemotherapy, and immunotherapy in malignant tumor treatment. *ACS Applied Bio Materials* 2019;**2**:874−83.
25. Emens LA, Middleton G. The interplay of immunotherapy and chemotherapy: harnessing potential synergies. *Cancer Immunol Res* 2015;**3**:436−43.
26. Cheng Y, Weng S, Yu L, Zhu N, Yang M, Yuan Y. The role of hyperthermia in the multidisciplinary treatment of malignant tumors. *Integr Canc Ther* 2019;**18**. 1534735419876345.
27. Singh A, Jain S, Sahoo SK. Magnetic nanoparticles for amalgamation of magnetic hyperthermia and chemotherapy: an approach towards enhanced attenuation of tumor. *Mater Sci Eng C Mater Biol Appl* 2020;**110**:110695.
28. Zheng Y, Cheng Y, Chen J, Ding J, Li M, Li C, et al. Injectable hydrogel-microsphere construct with sequential degradation for locally synergistic chemotherapy. *ACS Appl Mater Interfaces* 2017;**9**:3487−96.
29. Yu S, He C, Chen X. Injectable hydrogels as unique platforms for local chemotherapeutics-based combination antitumor therapy. *Macromol Biosci* 2018;**18**:e1800240.
30. Zhuang B, Chen T, Xiao Z, Jin Y. Drug-loaded implantable surgical cavity-adaptive hydrogels for prevention of local tumor recurrence. *Int J Pharm* 2020;**577**:119048.
31. Santhanam S, Liang J, Baid R, Ravi N. Investigating thiol-modification on hyaluronan *via* carbodiimide chemistry using response surface methodology. *J Biomed Mater Res A* 2015;**103**:2300−8.
32. Pu Y, Chen Y, Nguyen T, Xu CF, Zang L, Sosic Z, et al. Application of a label-free and domain-specific free thiol method in monoclonal antibody characterization. *J Chromatogr B* 2019;**1114−1115**:93−9.
33. Xu X, Bai B, Wang H, Suo Y. A near-infrared and temperature-responsive pesticide release platform through core−shell polydopamine@PNIPAm nanocomposites. *ACS Appl Mater Interfaces* 2017;**9**:6424−32.

34. Li W, Liu Z, Liu C, Guan Y, Ren J, Qu X. Manganese dioxide nanozymes as responsive cytoprotective shells for individual living cell encapsulation. *Angew Chem Int Ed Engl* 2017;**56**:13661−5.
35. Zhang M, Li M, Du L, Zeng J, Yao T, Jin Y. Paclitaxel-in-liposome-in-bacteria for inhalation treatment of primary lung cancer. *Int J Pharm* 2020;**578**:119177.
36. Burdick JA, Prestwich GD. Hyaluronic acid hydrogels for biomedical applications. *Adv Mater* 2011;**23**:H41−56.
37. He M, Sui J, Chen Y, Bian S, Cui Y, Zhou C, et al. Localized multidrug co-delivery by injectable self-crosslinking hydrogel for synergistic combinational chemotherapy. *J Mater Chem B* 2017;**5**:4852−62.
38. Tejido-Rastrilla R, Ferraris S, Goldmann WH, Grunewald A, Detsch R, Baldi G, et al. Studies on cell compatibility, cntibacterial behavior, and zeta potential of Ag-containing polydopamine-coated bioactive glass-ceramic. *Materials* 2019;**12**:500.
39. Wang B, Qiao C, Gao X, Yang X, Li Y, Li T. Rheological properties of *N*-[(2-hydroxyl)-propyl-3-trimethyl ammonium] chitosan chloride. *Carbohydr Polym* 2017;**171**:50−8.
40. Zhang H, Wang X, Wang P, Liu R, Hou X, Cao W, et al. One-pot synthesis of biodegradable polydopamine-doped mesoporous silica nanocomposites (PMSNs) as pH-sensitive targeting drug nanocarriers for synergistic chemo-photothermal therapy. *RSC Adv* 2018;**8**:37433−40.
41. Jia L, Han F, Wang H, Zhu C, Guo Q, Li J, et al. Polydopamine-assisted surface modification for orthopaedic implants. *J Orthop Translat* 2019;**17**:82−95.
42. Zhao Z, Chen C, Wu W, Wang F, Du L, Zhang X, et al. Highly efficient photothermal nanoagent achieved by harvesting energy *via* excited-state intramolecular motion within nanoparticles. *Nat Commun* 2019;**10**:768.
43. Zhuang WR, Wang Y, Cui PF, Xing L, Lee J, Kim D, et al. Applications of pi−pi stacking interactions in the design of drug-delivery systems. *J Control Release* 2019;**294**:311−26.
44. Zhang L, Yang P, Guo R, Sun J, Xie R, Yang W. Multifunctional mesoporous polydopamine with hydrophobic paclitaxel for photoacoustic imaging-guided chemo-photothermal synergistic therapy. *Int J Nanomed* 2019;**14**:8647−63.
45. Wang Y, Xiang Y, Xin VW, Wang XW, Peng XC, Liu XQ, et al. Dendritic cell biology and its role in tumor immunotherapy. *J Hematol Oncol* 2020;**13**:107.
46. Zhang N, Song J, Liu Y, Liu M, Zhang L, Sheng D, et al. Photothermal therapy mediated by phase-transformation nanoparticles facilitates delivery of anti-PD1 antibody and synergizes with antitumor immunotherapy for melanoma. *J Control Release* 2019;**306**:15−28.
47. Beheshti A, Wage J, McDonald JT, Lamont C, Peluso M, Hahnfeldt P, et al. Tumor-host signaling interaction reveals a systemic, age-dependent splenic immune influence on tumor development. *Oncotarget* 2015;**6**:35419−32.
48. Chen W, Qin M, Chen X, Wang Q, Zhang Z, Sun X. Combining photothermal therapy and immunotherapy against melanoma by polydopamine-coated Al_2O_3 nanoparticles. *Theranostics* 2018;**8**:2229−41.
49. Yang W, Zhang F, Deng H, Lin L, Wang S, Kang F, et al. Smart nanovesicle-mediated immunogenic cell death through tumor microenvironment modulation for effective photodynamic immunotherapy. *ACS Nano* 2020;**14**:620−31.
50. Jaime-Sanchez P, Uranga-Murillo I, Aguilo N, Khouili SC, Arias MA, Sancho D, et al. Cell death induced by cytotoxic $CD8^+$ T cells is immunogenic and primes caspase-3-dependent spread immunity against endogenous tumor antigens. *J Immunother Cancer* 2020;**8**:e000528.
51. Wang R, He Z, Cai P, Zhao Y, Gao L, Yang W, et al. Surface-functionalized modified copper sulfide nanoparticles enhance checkpoint blockade tumor immunotherapy by photothermal therapy and antigen capturing. *ACS Appl Mater Interfaces* 2019;**11**:13964−72.
52. Ge R, Liu C, Zhang X, Wang W, Li B, Liu J, et al. Photothermal-activatable Fe_3O_4 superparticle nanodrug carriers with PD-L1 immune checkpoint blockade for anti-metastatic cancer immunotherapy. *ACS Appl Mater Interfaces* 2018;**10**:20342−55.